IOP Publishing Journal of Physics: Condensed Matter
J. Phys.: Condens. Matter **33** (2021) 115901 (12pp) https://doi.org/10.1088/1361-648X/abd33b

Efficient approaches to solutions of partition function for condensed matters

Bo-Yuan Ning[1], Le-Cheng Gong[2,3], Tsu-Chien Weng[4,*] and Xi-Jing Ning[2,3,*]

[1] Center for High Pressure Science & Technology Advanced Research, Shanghai, 202103, People's Republic of China
[2] Institute of Modern Physics, Fudan University, Shanghai, 200433, People's Republic of China
[3] Applied Ion Beam Physics Laboratory, Fudan University, Shanghai, 200433, People's Republic of China
[4] School of Physical Science and Technology, ShanghaiTech University, Shanghai 201210, People's Republic of China

E-mail: wengzq@shanghaitech.edu.cn and xjning@fudan.edu.cn

Received 8 September 2020, revised 29 November 2020
Accepted for publication 14 December 2020
Published 29 December 2020

Abstract

The key problem of statistical physics standing over one hundred years is how to exactly calculate the partition function (or free energy), which severely hinders the theory to be applied to predict the thermodynamic properties of condensed matters. Very recently, we developed a direct integral approach (DIA) to the solutions and achieved ultrahigh computational efficiency and precision. In the present work, the background and the limitations of DIA were examined in details, and another method with the same efficiency was established to overcome the shortage of DIA for condensed system with lower density. The two methods were demonstrated with empirical potentials for solid and liquid cooper, solid argon and C_{60} molecules by comparing the derived internal energy or pressure with the results of vast molecular dynamics simulations, showing that the precision is about ten times higher than previous methods in a temperature range up to melting point. The ultrahigh efficiency enables the two methods to be performed with *ab initio* calculations and the experimental equation of state of solid copper up to $\sim$ 600 GPa was well reproduced, for the first time, from the partition function via density functional theory implemented.

Keywords: statistical physics, partition function, free energy calculation

Supplementary material for this article is available online

(Some figures may appear in colour only in the online journal)

1. Introduction

The widely used *ab initio* calculations may provide useful information for the material designs, while the results are in principle reliable for systems at zero Kelvin, and may lead to large deviations from finite-temperature cases. Actually, at room temperature or high temperature zone, statistical physics brings a promising prospect that all the thermodynamic properties of macroscopic matter can be thoroughly predicted without any empirical data as long as the partition function (PF) or free energy (FE) can be calculated precisely [1]. Unfortunately, it is yet quite difficult for the theory to be applied practically in condensed matter systems to determine the equation of states (EOSs) [2, 3], the condition of solid–solid or solid–liquid phase transitions [4–6], or the probability of isomers of larger molecules at arbitrary temperatures.

The problem standing in front of statistical physics stems from the fact that exact solution of the PF for a condensed system consisting of N particles involves a $3N$-fold configurational integral (CI), which goes far beyond the capacity

* Authors to whom any correspondence should be addressed.

of modern computers. For an example, solving the 180-fold integral of the PF for a C_{60} molecule by the conventional integral algorithms using an empirical potential would cost at least 10^{100} years even if a cutting-edge supercomputer with $\sim 10^{16}$ FP64 operations per second is employed.

In the past century, a lot of efforts have been contributed to approaching the problems for solving PF. Among these attempts, the cluster expansion (CE) of CI proposed by Mayer in 1941 [7] should be an efficient analytical approach, and has been continuously developed up to present [8]. Although CE has been applied in several aspects [6, 8–10], for condensed matters, the exact CE would exhibit non-physical behaviors [6]. Moreover, it should be pointed out that CE concerns only pairwise additive potentials, which are usually suitable for gas but cannot well describe the many-body interactions between atoms of metals, alloys or ceramics. Even so, the integrals of high-order CE are yet as complex as the 3*N*-fold CI.

Alternative routes are resorted to numerical molecular simulations, that is, either on the basis of molecular dynamics (MD) simulation to trace the trajectories by integrating Newton's equation of motion, or, in a manner of Monte Carlo (MC) formalism to sample the microstates in phase space by stochastic walks. The long-standing challenge in face of both MD and MC is how to protect the simulations from being trapped in a local FE minimum, or in other words, how to find those microstates that have major contributions to the PF within a limited simulation period [11]. Metadynamics was put forward [12, 13] to solve the problem in the way of MD simulations by finding a set of order parameters, the so-call collective variables (CVs), so that the dynamics run in the phase space of CVs are able to escape from the FE wells more easily. The prominent success is that the sampling efficiency would be greatly enhanced if both the selected CVs and the predefined bias function are appropriately chosen [14]. It should be noted that the sampling efficiency would be no much different from that of conventional MD simulations if inappropriate CVs are selected [15, 16]. Nowadays, the major researches are focusing on the methologies of choosing CVs [17–19] and constructing the bias potential [20].

Following the path of MC sampling, progress has been made in evaluations of the relative difference of PF (or FE) [21–23], and more efforts are being paid to the density of state (DOS) of potential energies to calculate absolute PF [24–26]. The advantage of DOS calculation lies in its independence of temperature and is able to solve out all the thermal properties of interest under any conditions instantly. Among various methods, Wang–Landau sampling [24] was the first breakthrough that the utilized biased weights make it possible to help the sampling climb over high FE barriers and visit rare states with equal probability. In spite of its special benefits for low-temperature cases, the method does not exhibit remarkable improvement in terms of sampling efficiency [27]. Recently developed nested sampling (NS) may be state-of-the-art technique [28], which aims at uniformly sampling a series of fixed fractions partitioned by potential energies in configurational space [29, 30] and has been successfully applied in several systems described by empirical potentials [31–41]. Despite of its improved 2–3 orders of computational efficiency, the affordable system scale of NS can be hardly over several hundred particles because of the large amount of sampling procedures, even if the empirical pairwise potentials are employed.

It is worth noting that the CI for a system consisting of N particles is made up of contributions from all the microstates of the configurational space, which can be divided as gas, liquid and solid regions. So, the total CI of a system, $\mathcal{Q}_T$, is the sum of partial CIs, $\mathcal{Q}_g$, $\mathcal{Q}_l$, $\mathcal{Q}_s$ belonged to the gas, liquid and solid states respectively. According to statistical theory, the probability for the system with given volume and temperature staying in the gas, liquid or solid states, as well as the probability for the solid being in different structures S_1, $S_2\ldots$, can be precisely determined by the ratio of partial CIs, $\mathcal{Q}_\alpha/\mathcal{Q}_\beta$, as long as $\mathcal{Q}_g$, $\mathcal{Q}_l$, $\mathcal{Q}_s$ ($\mathcal{Q}_{s_1}$, $\mathcal{Q}_{s_2}\ldots$) are obtained. For instance, to see the probabilities for C_{60} molecules existing in a perfect football structure or a defective one at a given temperature, or a metal existing in fcc or bcc structure with given volume and temperature, etc, it is only necessary to calculate the partial CIs of these specific structures without calculating the total CI of the system.

Very recently, instead of tackling CI by means of CE, MD or MC, we have put forward a completely different method, named direct integral approach (DIA) based on our *reinterpretation* of original sense of integral [42, 43], to solve the CI for liquid and solid with specific structures. The method improves the computational efficiency by four orders than state-of-the-art algorithm and has been successfully applied to calculate the FE of 2D materials as graphene, γ-grapyne, silicene [42], and EOS of solid argon (Ar) [43]. The accuracy was compared with NS [43], showing that the computational precision of DIA is about ten times higher for condensed systems. In the present work, we fully examined the background and limitations of DIA, showing that its accuracy gets gradually lower as the density decreasing. In order to cover the shortage, we proposed another method called effective entropy approach (EEA), which stems from the fact that the contribution of interacting particles to entropy is similar to that of non-interaction particles except that the movable space for the interacting particles is reduced by the interactions. For testing the above analytical results stringently, several empirical potentials, such as tight-binding (TB), Lennard-Jones (L-J) and Brenner were employed to calculate the PF for solid and liquid copper (Cu), solid Ar, C_{60} clusters, and the derived internal energy and EOSs were compared to vast MD simulations, showing the calculation precision is about ten times higher than state-of-the-art technique. It should be stressed that tests by MD simulations using the same interaction potential as used in calculations of PF are much more rigorous than those by experimental measurements, though most methods for solving PF are mainly tested by direct comparisons with experiments. This argument comes from the fact that in most cases the interaction potential (even gained from *ab initio* methods) used for solving PF are not precise for the realistic systems and may lead to the theoretical results in agreement with experimental measurements even though the methods for solving PF are not accurate. Thanks to the ultrahigh computational efficiency of the two methods, we successfully implemented density

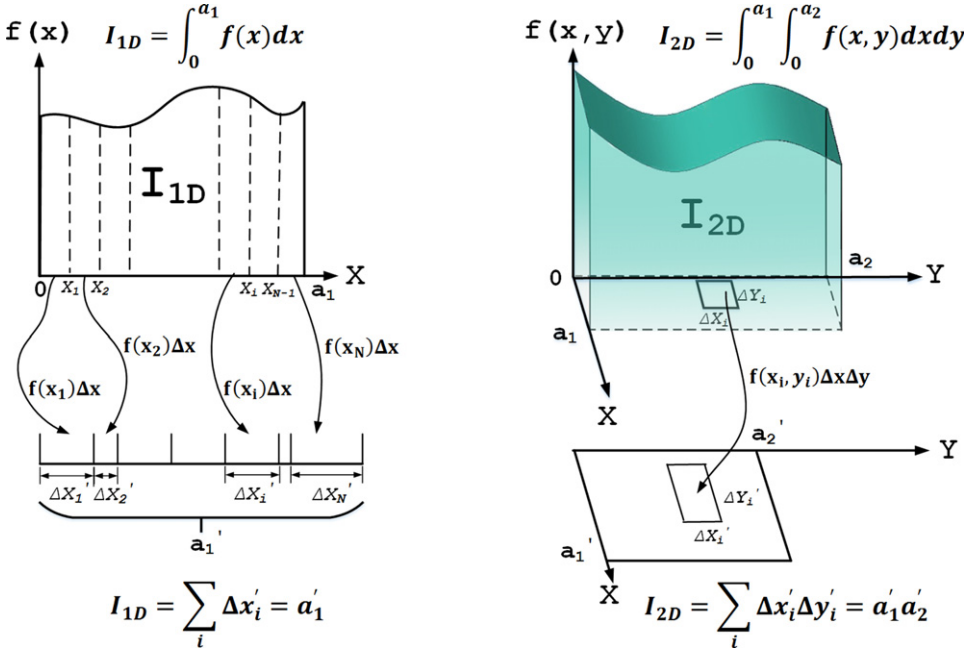

Figure 1. A one-fold integral can be interpreted as an effective length (left) and a two-fold integral equals to an effective area (right).

functional theory (DFT) calculations of the PF of Cu to produce its EOS up to ultrahigh-pressure zone.

2. Theoretical model

2.1. Direct integral approach

The original sense of one-fold (1D) integral $I_{1D} = \int_0^{a_1} f(x)\mathrm{d}x$ is interpreted as the sum of infinite number of rectangles with area $A_i = f(x_i)\Delta x$, and $I_{1D} = \lim_{\Delta x\to 0}\sum_i A_i$. Here, we interpret the integral from a different angle: the length element Δx at x_i is modulated by $f(x_i)$ to be a new length element $\Delta x_i' = f(x_i)\Delta x$ and $I_{1D} = \sum_i \Delta x_i'$. In other words, the 1D integral is a summation of length elements instead of area elements and equals to an effective length, a_1', of a_1 (see left in figure 1). Similarly, a two-fold integral $I_{2D} = \int_0^{a_1}\int_0^{a_2}\mathrm{d}x\ \mathrm{d}y f(x,y)$ equals to an effective area, $a_1'\cdot a_2'$, of $a_1\cdot a_2$ because the area element $\mathrm{d}s = \mathrm{d}x\mathrm{d}y$ is enlarged (or shrunk) by $f(x,y)$ giving rise to an effective area element $\mathrm{d}s' = f(x,y)\mathrm{d}x\mathrm{d}y$ (see right in figure 1). Followed by this notion, an N-fold integral $I_{ND} = \int_0^{a_1}\int_0^{a_2}\ldots\int_0^{a_N}\mathrm{d}q_1\ \mathrm{d}q_2\ldots\mathrm{d}q_N f(q_1,q_2\ldots q_N)$ equals to an effective volume, $a_1'\cdot a_2'\ldots a_N'$.

When the integrand $f(q_1,q_2\ldots q_N)$ is in a form of $\exp[-U(q_1,q_2\ldots q_N)]$ with $U(q_1,q_2\ldots q_N)$ being positive definite within the integral domain and having minimum at the origin ($U(0)=0$), the effective length of a_i is defined as

$$a_i' = \int_0^{a_i} \exp[-U(0\ldots q_i\ldots 0)]\mathrm{d}q_i, \quad (i = 1,2\ldots N) \quad (1)$$

and the effective volume approximates to $\prod_{i=1}^{N} a_i'$, i.e.,

$$I_{ND} \simeq \prod_{i=1}^{N} a_i'. \quad (2)$$

We start the proof of equation (2) from a 2D integral,

$$I_{2D} = \int_0^{a_1}\mathrm{d}x\int_0^{a_2}\mathrm{d}y\ \mathrm{e}^{-U(x,y)}, \quad (3)$$

where $U(x,y)$ is positive definite within the integral domain, $0\leqslant x\leqslant a_1, 0\leqslant y\leqslant a_2$, on which we define a map of x and y,

$$X'(x) = \int_0^x \mathrm{e}^{-U(\xi,0)}\ \mathrm{d}\xi,$$
$$Y'(y) = \int_0^y \mathrm{e}^{-U(0,\xi)}\ \mathrm{d}\xi. \quad (4)$$

So $X'(0)=0$, $Y'(0)=0$. The effective length of a_1 and a_2 is defined by

$$a_1' = \int_0^{a_1} \mathrm{e}^{-U(\xi,0)}\ \mathrm{d}\xi,$$
$$a_2' = \int_0^{a_2} \mathrm{e}^{-U(0,\xi)}\ \mathrm{d}\xi. \quad (5)$$

Inserting equation (4) into equation (3) yields

$$I_{2D} = \int_0^{a_1'}\mathrm{d}X'\int_0^{a_2'}\mathrm{d}Y'\ \mathrm{e}^{-F(X',Y')} \quad (6)$$

with

$$F(X',Y') = U(x(X'),y(Y')) - U(x(X'),0) - U(0,y(Y')), \quad (7)$$

which can be expanded in Taylor series as

$$F(X',Y') = F(0,0) - \left.\frac{\partial F}{\partial X'}\right|_0 \Delta X' - \left.\frac{\partial F}{\partial Y'}\right|_0 \Delta Y' \ldots \quad (8)$$

If $U(x,y)$ has a minimum at the origin ($x=0$, $y=0$) and $U(0,0)=0$, then $F(0,0)=0$, $\left.\frac{\partial F}{\partial X'}\right|_0 = \left.\frac{\partial F}{\partial Y'}\right|_0 = 0$ and thus the value of $F(X',Y')$ is close to zero in the neighborhood of $(0,0)$.

Since $U(x, y)$ is positive definite, a' and b' are small, and the integral domain of equation (6) is a small area around the origin, we obtain that

$$I_{2D} \simeq a'_1 a'_2. \tag{9}$$

Similarly, the solution of $\prod_i^N \int_0^{a_i} \mathrm{d}q_i \exp[-U(q_1, q_2 \ldots q_N)]$ is equation (2) as long as $U(q_1, q_2 \ldots q_N)$ is positive definite and has a minimum at the origin ($U(0) = 0$). In this way, the N-fold integral is turned into one-fold integral, and the method is named as DIA.

It should be stressed that the Taylor expansion in equation (8) validates only within the neighborhood of the origin of U, indicating an additional condition for validation of equation (9) (or equation (2)) is that a'_i should be small enough. In some cases, although the function $U(q_1, q_2 \ldots q_N)$ meets the basic demands as being positive definite and minimum at the origin, such as $U(q_1, q_2 \ldots q_n) = \prod_i^N q_i^2$, the effective length a'_i is as large as a_i, and therefore equation (2) or equation (9) is no longer valid. Fortunately, such cases can hardly happen when DIA is applied to solve the CI for realistic physical systems, which can been seen from the followed equation (10).

Now consider CI for a continuum system consisting of N particles in liquid or solid state at a given temperature T,

$$\mathcal{Q} = \int \mathrm{d}q^{3N} \exp[-\beta U(q^{3N})], \tag{10}$$

where $\beta = 1/k_B T$ with k_B the Boltzmann constant, $q^{3N} = \{q_1, q_2 \ldots q_{3N}\}$ the Cartesian coordinates of particles and $U(q^{3N})$ the potential function. Although the integrand is in the same form as required by equation (2), it may not be positive definite or have no minimum at the origin ($q^{3N} = 0$). Letting the set $Q^{3N} = \{Q_1, Q_2 \ldots Q_{3N}\}$ be the coordinates of particles in state of the lowest potential energy U_0, we may introduce a function

$$U'(q'^{3N}) = U(q^{3N}) - U_0, \tag{11}$$

where $q'_i = q_i - Q_i$. By inserting equation (11) into equation (10), we obtain

$$\mathcal{Q} = \mathrm{e}^{-\beta U_0} \int \mathrm{d}q'^{3N} \exp[-\beta U'(q'^{3N})]. \tag{12}$$

Clearly, $U'(q'^{3N})$ is positive definite within all the integral domain and has minimum at the origin ($U'(0) = 0$). According to equation (2), the integral in equation (12) equals to an effective $3N$-fold volume,

$$\mathcal{Q} = \mathrm{e}^{-\beta U_0} \prod_{i=1}^{3N} \mathcal{L}_i, \tag{13}$$

where the effective length $\mathcal{L}_i$ on the ith degree of freedom is defined as

$$\mathcal{L}_i = \int \mathrm{e}^{-\beta U'(0 \ldots q'_i \ldots 0)} \mathrm{d}q'_i. \tag{14}$$

For homogeneous systems with certain geometric symmetry, such as perfect one-component crystals, all the particles are geometrically equivalent and U' felt by one particle moving along q'_x may be the same as the one along q'_y (or q'_z). In such a case, equation (13) turns into

$$\mathcal{Q} = \mathrm{e}^{-\beta U_0} \ \mathcal{L}^{3N}, \tag{15}$$

where $\mathcal{L}$ is the effective length determined by equation (14). Otherwise, it is needed to calculate the effective length, $\mathcal{L}_x$, $\mathcal{L}_y$, $\mathcal{L}_z$ by equation (14) of an arbitrary particle, and equation (13) turns into

$$\mathcal{Q} = \mathrm{e}^{-\beta U_0} (\mathcal{L}_x \mathcal{L}_y \mathcal{L}_z)^N. \tag{16}$$

The procedure can be extended to systems composed of different particle species by calculating the effective length of each species respectively.

For inhomogeneous systems, such as defects or interfaces existed, particles may be grouped into M sets numbered by I with each containing N_I equivalent particles, and the CI becomes

$$\mathcal{Q} = \mathrm{e}^{-\beta U_0} \prod_{I=1}^{M} [\mathcal{V}_I]^{N_I}, \tag{17}$$

where $\mathcal{V}_I = \int \mathrm{e}^{-\beta U'(x)} \mathrm{d}x \int \mathrm{e}^{-\beta U'(y)} \mathrm{d}y \int \mathrm{e}^{-\beta U'(z)} \mathrm{d}z$ denotes the effective volume of an arbitrary particle in the Ith set with Cartesian coordinates x, y, z.

It should be bore in mind that the above derived $\mathcal{Q}$ is the partial CI for a specific matter state, liquid or solid with given structure rather than the total CI resulted from all the microstates of the system in every state. For a given state, liquid, solid or cluster of an N-particle system, the first step of using DIA is to find the most stable structure (MSS) for determining U_0, which can be accomplished in principle by several well-developed methods, such as global optimizations [44–47] or dynamic damping [48, 49]. Actually, the MSS for crystals can be immediately obtained by placing the particles right at the lattice sites. Then, we move a particle along its one degree of freedom q'_i to obtain $U'(0 \ldots q'_i \ldots 0)$ while its other degrees of freedom q'_j and all the other particles are kept fixed.

It is clear from equation (14) that the effective length $\mathcal{L}_i$ would continue to be larger with increases of the temperature and decreases of the potential $U'(0 \ldots q'_i \ldots 0)$, the latter corresponding to the decreases of the density. According to the conditions for validation of equation (9) that a_i should be small enough, the accuracy of equation (13) will get worse as the temperature increasing and density decreasing. This tendency of DIA was confirmed by the comparisons with MD simulations in section 3.

At a first glance, DIA might be regarded as similar to the phonon model with quasi-harmonic approximation. In fact, performance of the two approaches is very different, which has been demonstrated by our very recent work [50] showing that the EOS of crystal Ar along the melting line with temperature up to 2600 K is well reproduced by DIA and MD but differs from the result of the phonon model by 20%.

2.2. Effective entropy approach

The work of Watanabe and Reinhardt [51] proved that the entropy of an interacting system would be the same as that of a

non-interacting system by adiabatically switching off the interparticle interactions, which gives us a hint that the entropy of a realistic system may be expressed in a way similar to that of a non-interaction system,

$$\mathcal{S}_{ig} = \frac{3}{2}Nk_{\mathrm{B}}\ \ln\ T + \frac{3}{2}Nk_{\mathrm{B}}\left(\frac{5}{3} + \ln\ \frac{2m\pi k_{\mathrm{B}}}{h^2}\right) + Nk_{\mathrm{B}}\ \ln\ \frac{V}{N}, \tag{18}$$

where V is the volume for the particles freely moving in.

For an interacting system, the PF can be written as

$$\mathcal{Z} = \frac{1}{N!}\left(\frac{2m\pi}{\beta h^2}\right)^{\frac{3}{2}N} \mathrm{e}^{-\beta U_0}\mathcal{Q}', \tag{19}$$

where $\mathcal{Q}' = \int \mathrm{d}q'^{3N}\ \exp[-\beta U'(q'^{3N})]$ (see equation (12) for details), and the entropy can be expressed via $\mathcal{S} = k_{\mathrm{B}}\left(\ln\ \mathcal{Z} - \beta\frac{\partial}{\partial\beta}\ \ln\ \mathcal{Z}\right)$ in terms of the effective volume V_{eff} as

$$\begin{aligned}\mathcal{S} &= \frac{3}{2}Nk_{\mathrm{B}}\ \ln\ T + \frac{3}{2}Nk_{\mathrm{B}}\left(\frac{5}{3} + \ln\ \frac{2m\pi k_{\mathrm{B}}}{h^2}\right) \\ &\quad + \left[Nk_{\mathrm{B}}\ \ln\ \frac{1}{N} + k_{\mathrm{B}}\left(\ln\ \mathcal{Q}' - \beta\frac{\partial}{\partial\beta}\ \ln\ \mathcal{Q}'\right)\right] \\ &= \frac{3}{2}Nk_{\mathrm{B}}\ \ln\ T + \frac{3}{2}Nk_{\mathrm{B}}\left(\frac{5}{3} + \ln\ \frac{2m\pi k_{\mathrm{B}}}{h^2}\right) \\ &\quad + Nk_{\mathrm{B}}\ \ln\ \frac{V_{\mathrm{eff}}}{N},\end{aligned} \tag{20}$$

where

$$V_{\mathrm{eff}} = \mathcal{Q}'^{\frac{1}{N}}\ \mathrm{e}^{\frac{\beta\tilde{U}'}{N}}, \tag{21}$$

and $\tilde{U}' = \int U'\ \mathrm{e}^{-\beta U'}\ \mathrm{d}q^{3N}$. Equation (20) implies that the contribution from interacting particles to entropy is the same as free particles except that the movable volume V for the free particles changes into V_{eff} for the interacting particles.

It is clearly that the changes of movable volume is just due to the interaction potential U' restricting the movable space of the interacting particles. For a non-interacting system, $U' = 0$, and according to equation (19), $\mathcal{Q}' = V^N$, so V_{eff} equals to V and equation (20) returns to equation (18), which indicates that V_{eff} should be mainly dependent on the potential U' felt by the particle. Based on above arguments, we made a conjecture that

$$V_{\mathrm{eff}}(\beta) = \int \mathrm{e}^{-\alpha U'(x,y,z)\beta}\ \mathrm{d}x\ \mathrm{d}y\ \mathrm{d}z, \tag{22}$$

where α is a universal dimensionless constant, and $U'(x, y, z)$ is the potential felt by an arbitrary particle moving in the system with other particles fixed. For one particle moving in a one-dimension potential $U'(x) = \frac{1}{2}ax^2$ or $U'(x) = a|x|$, where a is an arbitrary positive number, the PF $\mathcal{Z}$ can be analytically solved, and the entropy is $\mathcal{S} = k_{\mathrm{B}}\left(\ln\ \mathcal{Z} - \beta\frac{\partial}{\partial\beta}\ \ln\ \mathcal{Z}\right)$, which produces the exact effective V_{eff} via equation (20). The value of V_{eff} for the two potentials can be reproduced by equation (22) with $\alpha = 1/e$, showing that equation (22) validates for the two potentials.

Through equations (20) and (22), the entropy of any system $\mathcal{S}(\beta)$ can be obtained and further the PF, $\mathcal{Z}$, can be determined via $\mathcal{S}(\beta) = k_{\mathrm{B}}\left(\ln\ \mathcal{Z} - \beta\frac{\partial}{\partial\beta}\ \ln\ \mathcal{Z}\right)$ by (see derivations in appendix A)

$$\ln\ \mathcal{Z} = \beta\left(C_0 - \int_{\beta_0}^{\beta}\frac{\mathcal{S}'(\eta)}{\eta^2}\ \mathrm{d}\eta\right), \tag{23}$$

where $\mathcal{S}'(\eta) = \mathcal{S}(\eta)/k_{\mathrm{B}}$, and C_0 is a constant to be determined as follows. The internal energy E reads,

$$E = -\frac{\partial}{\partial\beta}\ \ln\ \mathcal{Z} = -C_0 + \frac{\mathcal{S}'(\beta_0)}{\beta_0} + \int_{\beta_0}^{\beta}\frac{1}{\eta}\,\mathrm{d}\mathcal{S}'(\eta), \tag{24}$$

and from equations (20) and (22), we get

$$\mathrm{d}\mathcal{S}'(\eta) = -\frac{3}{2}N\frac{1}{\eta}\,\mathrm{d}\eta + N\bar{U}'(\eta)\mathrm{d}\eta, \tag{25}$$

where $\bar{U}'(\eta) = \frac{\partial}{\partial\eta}\ \ln\ V_{\mathrm{eff}}(\eta)$. Insert equation (25) into equation (24), we obtain

$$E = -C_0 + \frac{\mathcal{S}'(\beta_0)}{\beta_0} + \frac{3N}{2}\left(\frac{1}{\beta} - \frac{1}{\beta_0}\right) - N\int_{\beta_0}^{\beta}\bar{U}'\frac{1}{\eta}\ \mathrm{d}\eta. \tag{26}$$

When $T \to 0$ ($\beta \to \infty$), $E \to U_0$, C_0 is determined as

$$C_0 = -U_0 + \frac{\mathcal{S}'(\beta_0)}{\beta_0} + \frac{3N}{2}\left(\frac{1}{\beta} - \frac{1}{\beta_0}\right) - N\int_{\beta_0}^{\beta}\bar{U}'\frac{1}{\eta}\ \mathrm{d}\eta. \tag{27}$$

To this far, the PF can be solved to produce all the thermodynamic functions, such as internal energy and pressure,

$$\begin{aligned}E &= U_0 + \frac{3}{2}Nk_{\mathrm{B}}T + N\int_0^T \bar{U}'(\xi)\frac{1}{\xi}\ \mathrm{d}\xi, \\ P &= -\frac{\partial E}{\partial V} + Nk_{\mathrm{B}}T\frac{1}{V_{\mathrm{eff}}}\frac{\partial V_{\mathrm{eff}}}{\partial V}.\end{aligned} \tag{28}$$

If a system contains M kinds of particles, which have different potential U' because of their different surroundings, such as in liquid or amorphous solid, the effective volume is defined by

$$V_{\mathrm{eff}} = \frac{1}{M}\sum_{I=1}^{M} V_{\mathrm{eff}}^I, \tag{29}$$

where V_{eff}^I is the effective volume of an arbitrary atom in the Ith kinds and thus has the similar expression as equation (22). With the same procedures as above, E and P are expressed as

$$\begin{aligned}E &= U_0 + \frac{3}{2}Nk_{\mathrm{B}}T + N\sum_{I=1}^{M}\int_0^T \bar{U}'^I\frac{1}{\xi}\ \mathrm{d}\xi, \\ P &= -\frac{\partial E}{\partial V} + Nk_{\mathrm{B}}T\frac{1}{\sum_{I=1}^{M} V_{\mathrm{eff}}^I}\frac{\partial\sum_{I=1}^{M} V_{\mathrm{eff}}^I}{\partial V},\end{aligned} \tag{30}$$

where

$$\bar{U}'^I = \frac{1}{\sum_{I=1}^{M} V_{\mathrm{eff}}^I}\int(\alpha U'^I)\mathrm{e}^{-\alpha U'^I\beta}\ \mathrm{d}x. \tag{31}$$

In the above model named by EEA, the key step is solving the 3-fold integral of V_{eff} (equation (22)), which would lead to

much computational cost. An approximation may be made by separating the 3-fold integral into three one-fold integrals as

$$V_{\text{eff}} = \int \mathrm{e}^{-\alpha U'(x,0,0)\beta}\,\mathrm{d}x \int \mathrm{e}^{-\alpha U'(0,y,0)\beta}\,\mathrm{d}y \times \int \mathrm{e}^{-\alpha U'(0,0,z)\beta}\,\mathrm{d}z. \tag{32}$$

In this way, the main calculation task for EEA is nearly the same as that for DIA, details of which can been seen in the last paragraph of section 2.1. Preliminary MD simulations of solid Cu showed that the value of α of EEA should be set as 0.17, which is about an half of the value $1/e$ for one particle moving in one-dimensional potential, and in the following applications of EEA, the value of α is always set to be 0.17.

3. Results and discussions

To test the accuracy of DIA and EEA, we may perform *ab initio* calculations of $U'(0\ldots q_i'\ldots 0)$ on some realistic systems and compare the derived results with related experiments. However, results from first principle calculations may be strongly dependent on the specific algorithms, such as different types of exchange–correlation functions in DFT, and the experimental data are usually insufficient for extensive comparisons. In such cases, even if the results derived from the PF are in good agreement with the experimental data, it would be yet doubted of the accuracy of DIA or EEA. In order to have a stringent test, we fist employed empirical potentials to calculate the PF of several systems by DIA and EEA, and the derived internal energy and EOS were compared with MD simulations using the same potentials. The results of PF were also compared with experimental data, showing that the TB potential is suitable for solid Cu with ordinary density and L-J potential is excellent for Ar. Furthermore, DIA and EEA were performed with *ab initio* calculations for solid Cu and the derived EOS coincides well with experimental data, especially at high-pressure zone.

3.1. For solid and liquid copper

Considering the huge computational cost of the MD simulations, the number of Cu atoms in our model is limited to 4000, which were confined in a cubic box with periodic boundary condition applied. The TB potential [52] was employed to describe the interatomic interactions. For solid Cu, the MSS was found by arranging the atoms at the fcc lattice sites. In consideration of the Fm−3m symmetry of fcc lattice, the Cartesian Z-axis of atoms is set to [001] direction so that the potential U' felt by an atom moving along the X-axis (or Y-axis) is the same as the one along the Z-axis. To obtain $U'(Z)$, the Z coordinate of the geometry-center atom was changed step by step with its X and Y coordinates fixed to record the potential energies, during which all the other atoms stay fixed as well.

For the liquid Cu, the amorphous structure was prepared by heating the solid Cu up to 2.5×10^4 K in MD simulation to generate a uniform distribution of atoms, and a damped trajectory method [48] was used to determine the MSS and potential energy U_0 (see details in supplementary information (https://stacks.iop.org/JPCM/33/115901/mmedia)).

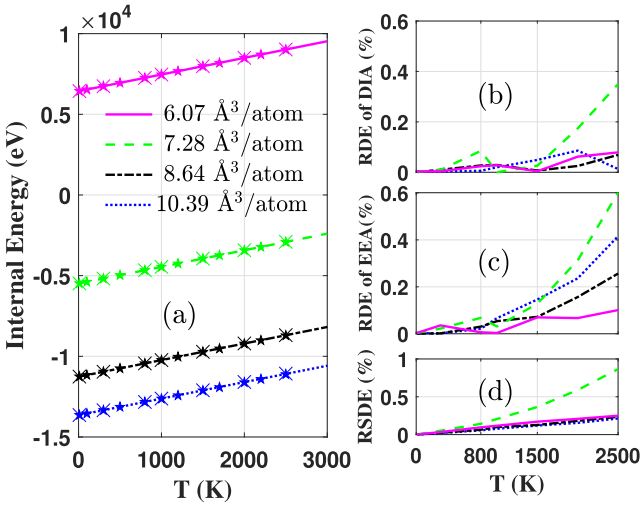

Figure 2. For solid Cu with atomic volumes of 6.07, 7.28, 8.64 and 10.39 Å^3/atom (colored in magenta, green, black and blue respectively), the internal energies obtained from DIA (lines), EEA (pentagons) and MD simulations (crosses) (a), and the relative difference between the MD simulations and DIA (b) as well as EEA (c), and the relative standard deviations (RSDE) of MD simulations (d), where different colors correspond to different atomic volumes shown in (a).

Different from the cases in the solid Cu, the potential U' felt by a liquid atom moving along the X-, Y- or Z-axis may not be the same, so $U'(x)$, $U'(y)$ and $U'(z)$ for a single atom located in the center region were calculated respectively and equation (16) was applied to obtain the CI by DIA. To apply EEA, we chose 20 atoms in the center region of the relaxed MSS and equation (30) was used to calculate the CI.

Common procedures for MD simulations of a canonical ensemble [49] was employed to produce the internal energy (E) and pressure (P) of the systems contacted with a thermal bath at given temperatures, and the Verlet algorithm [53] was employed for integrating the equations of motion with a time step of 0.1 fs and 0.01 fs for the solid and liquid respectively. We first fully relaxed the systems for 10^5 steps, and ran another 10^5 (or 10^6) steps to record the values of E and P for the solid (or liquid). Attentions have to be paid that the commonly used Virial equations [54] are inaccurate to compute pressure in the case of many-body potential with periodic boundary condition applied [55, 56], and we employed the method proposed by Tsai [57] that considers stress and momentum flux across an area for conducting the statistic of P.

For the solid systems with atomic volume ranging from 6.07 to 10.39 Å^3/atom (colored in magenta, green, black and blue respectively in figures 2 and 3), the internal energy E_{PF} and pressure P_{PF} derived from the PF obtained by DIA or EEA are in excellent agreement with those (E_{MD} and P_{MD}) obtained by MD simulations at temperatures from 10 K to 2500 K (figures 2 and 3). When the temperatures of the systems, except for the one of an atomic volume of 7.28 Å^3/atom, are below 1500 K, the relative difference of internal energy (RDE $= |(E_{\text{PF}} - E_{\text{MD}})/E_{\text{MD}}|$) of DIA is less than 0.03% (figure 2(b)), while for EEA, the RDE is less than 0.09% (figure 2(c)). As the temperature rises up to 2500 K, the

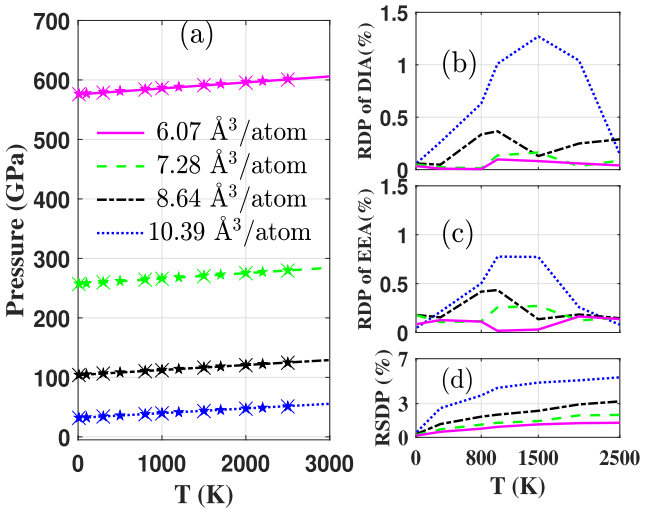

Figure 3. Similar to figure 2, the pressure obtained from DIA (lines), EEA (pentagons) and MD simulations (crosses) (a), and the relative difference between the MD and DIA (b) as well as EEA (c), and the relative standard deviations (RSDP) of MD simulations (d).

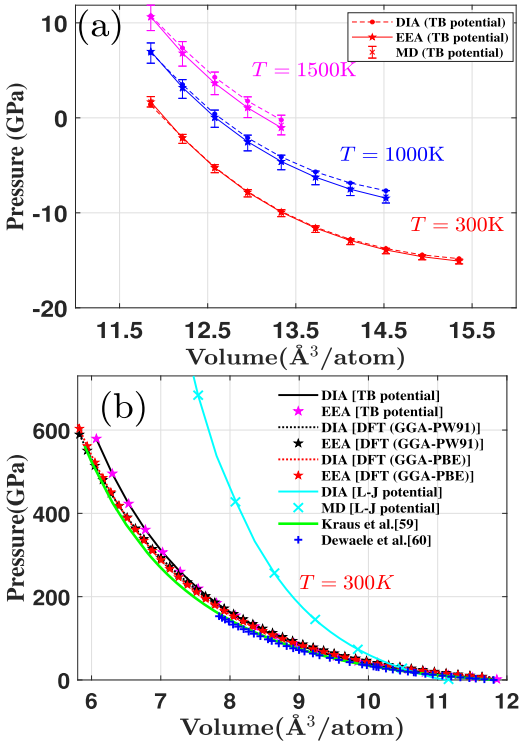

Figure 4. (a) Isothermal EOSs pressure obtained by DIA (solid circles), EEA (pentagons) and MD simulations (crosses) for solid Cu with atomic volumes larger than 11.5 Å^3/atom at 300 K (colored in red), 1000 K (colored in blue) and 1500 K (colored in magenta). The error bars stand for the standard deviations of MD simulations. (b) The experimental isothermal EOSs of solid Cu at 300 K with atomic volume smaller than 12 Å^3/atom, and those obtained by DIA and EEA using different potentials.

difference gets a bit larger and the maximum is 0.35% for DIA and 0.6% for EEA, which should be attributed to the statistical fluctuations of MD simulations because the relative standard deviations of internal energy (RSDE) increases by several times (figure 2(d)). In any case, the RDE of both the two methods is well within the RSDE of the MD simulations, while DIA works a little better. It is easy to understand why the RSDE of MD and the RDE of DIA or EEA for the system with atomic volume 7.28 Å^3/atom (green color in figure 2) are obviously larger, because the absolute value of the internal energy is relatively small. On the pressure, the overall relative difference of pressure (RDP $= |(P_{\rm PF} - P_{\rm MD})/P_{\rm MD}|$) is below 1% for both DIA (figure 3(b)) and EEA(figure 3(c)), which is a little larger than the RDE but still well covered by the relative standard deviations of pressure (RSDP) of MD, $\sim 3\%$, (figure 3(d)).

For the solid Cu system with atomic volume larger than 11.5 Å^3/atom, we calculated the isothermal EOSs at 300, 1000 and 1500 K by DIA, EEA and MD simulations, as shown in figure 4(a). For the EOS at 300 K, the pressure obtained by DIA and EEA coincides well with the results of MD simulations when the atomic volume is smaller than 15.35 Å^3/atom, which can been from the fact that the results derived from the two methods are within the fluctuations of MD simulations. Specifically, the RDP of EEA and DIA is about 1% and 2% respectively. When the atomic volume is larger than 15.3 Å^3/atom, the MD simulations showed that the systems cannot keep the crystalline structure and exhibit spatial holes [58], implying that solid-liquid phase transitions may take place, which would be extensively investigated by DIA and EEA in the near future. For the systems at 1000 K, the crystalline structure can be kept until the atomic volume reaches up to 14.52 Å^3/atom, below which the RDP of EEA and DIA is about 4% and 8% respectively. Although the RDP is obviously larger than that for 300 K, it is still smaller than the RSDP of the MD simulations. When the temperature was lift to 1500 K, the largest atomic volume for the crystalline structure reduced down to 13.33 Å^3/atom, and the RDP of DIA increases up to about three times larger than that of the EEA. Even so, the standard deviation of DIA from the MD simulation is still within the fluctuations.

The above results show that for the systems of large atomic volume, EEA works better than DIA, and DIA behaves worse and worse with increases of the atomic volume and temperature while EEA does not. This tendency is inevitable because the condition for validation of equation (15) (or equation (2)) in DIA is that the effective length, $\mathcal{L}_i$ (or a_i), should be small enough, while according to equation (14), $\mathcal{L}_i$ increases with rise of the temperatures ($\beta = 1/k_{\rm B}T$) and the atomic volume that determines the value of U_i'. This is also the reason why DIA works better for the atomic values smaller than 10.39 Å^3/atom (figures 2 and 3).

The experimental isothermal EOS [59, 60] for the solid Cu with atomic volume of 6–12 Å^3/atom at 300 K exhibits the same trend as those obtained by DIA and EEA using the TB potential (figure 4(b)). Although the pressures derived by DIA are in an excellent agreement with those by EEA, they are about 10% larger than the experimental data. This discrepancy should be attributed to the inaccuracy of the empirical potential because the MD simulations produced nearly the same results as DIA or EEA (the RDP is about 3%). By contrast, we also used the L-J potential [61] to calculate the EOS by DIA. Although the outcome coincides well with the

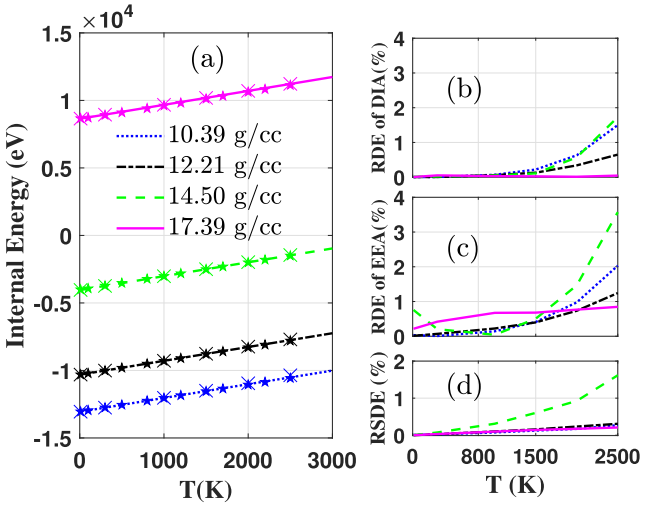

Figure 5. Similar to figure 2 except for the liquid state of the Cu systems with different mass densities.

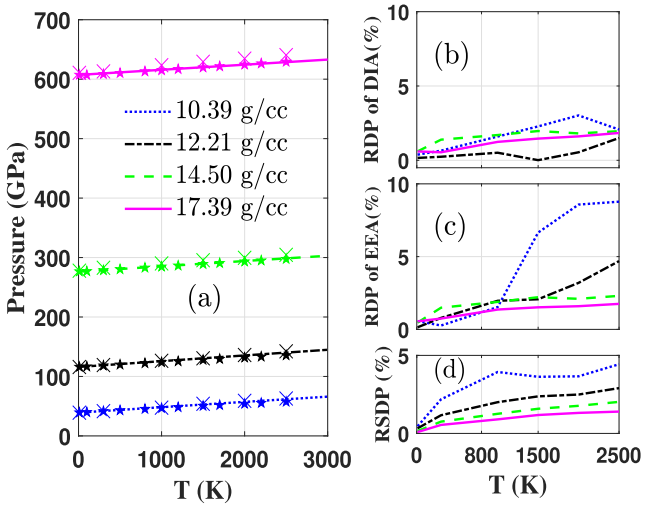

Figure 6. Similar to figure 3 except for the liquid state of the Cu systems with different mass densities.

corresponding MD simulations, it deviates much more from the experiments.

For acquiring a more accurate interatomic potential, we next used the DFT to calculate the U' in equations (14) or (32). All the DFT computations were conducted by the Vienna *ab initio* simulation package (VASP) 5.4.4 [62, 63], and two methods were employed, the ultrasoft pseudopotential (USPP) with Perdew–Wang 91 general gradient approximation (GGA-PW91) [64] for electronic exchange–correlation functional and the projector-augmented wave (PAW) formalism with Perdew–Burke–Ernzerhf general gradient approximation (GGA-PBE) [65]. 108 Cu atoms were considered in a $3 \times 3 \times 3$ supercell and a Γ-centered $4 \times 4 \times 4$ Monkhorst–Pack [66] k-point mesh was set to sample the Brillouin zone. In order to accelerate the speed of the DFT computation, the GPU supported VASP code [67–69] was used for the GGA-PW91, and the standard CPU-based VASP code was used for the GGA-PBE. The procedure to calculate the PF through DFT calculations is exactly the same as that of using empirical potentials, while the only difference is that, due to the large time-consumption of DFT self-consistent energy calculations, the sample points of U' curve by DFT are not as many as those by TB potentials. We calculated 20 potential-energy points for each U' curve within ~ 1 Å and then used standard interpolation algorithm to fit the curve of U' (see details in supplementary information). As can be seen in figure 4(b), the application of interatomic potential determined by DFT greatly improves the accuracy of the obtained EOS for both DIA and EEA, especially in the high-pressure zone (> 200 GPa). For instance, the pressure at 5.9 Å^3/atom obtained in reference [59] is 561.91 GPa, and it is 563.03 GPa and 562.88 GPa for DIA and EEA respectively with GGA-PW91 approach, and 574.76 GPa and 574.73 GPa with GGA-PBE approach. As we discussed above, it is the potential function that would largely affect the value of calculated PF when compared with experiments and both DIA and EEA are capable of implementing the more reliable *ab initio* calculations for the future PF computations.

For liquid Cu with mass density ranging from 10.39 to 17.39 g/cc, the internal energy and pressure of these disordered systems obtained by DIA and EEA are also in a good agreement with the MD simulations (figures 5 and 6). For DIA, the RDE and RDP are well smaller than the fluctuations of MD simulations, though they increase slowly with the temperatures up to 2500 K. Relatively, the RDE and RDP of EEA are a little larger and, in some cases, reach up to or beyond the boundary of MD simulations. The worse performance of EEA can be understood in consideration of the fact that the entropy equivalence of interacting systems to the non-interacting systems gets worse with increases of the mass density, which is rather high for the liquid Cu studied here. Fortunately, DIA works better and better with increasing of the mass density, which is inevitable because the higher mass density is the smaller effective length (cf equation (14)).

3.2. For solid argon

Pairwise additive L-J potential is widely used to describe the interatomic interaction in various kinds of condensed matter, so it is necessary to test the approaches to the PF of condensed systems with L-J potential. In this section, DIA and EEA were applied to solid Ar of fcc structure with L-J potential [54], which is believed to be a good approximation to realistic Ar atoms, and the derived pressure were compared with MD simulations, the results obtained by NS as well as available experimental data. The implementation details of DIA and EEA for the solid Ar are the same as those for solid Cu and the operation details of NS can be found in reference [43]. The MD simulations were conducted by using the large-scale atomic/molecular massively parallel simulator software package (LAMMPS) [70], and the Nose–Hoover algorithm [71] for canonical ensemble was employed with a time step of 1 fs to calculate the internal energy and pressure, the simulation process of which was firstly to relax the system at the given NVT condition for 5 ps and then continued to run the system for 20 ps.

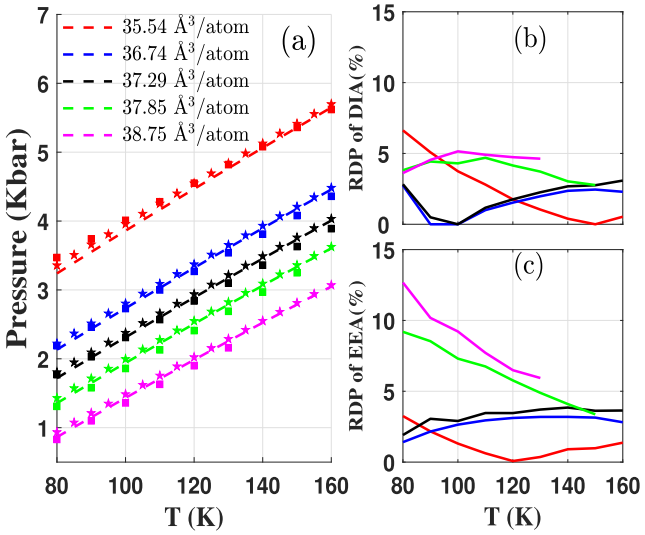

Figure 7. (a) Isochoric EOSs of solid Ar with atomic volumes of 35.54, 36.74, 37.29, 37.85 and 38.75 Å^3/atom, (colored in red, blue, black, green, magenta respectively) obtained by DIA (dashed lines) and EEA (pentagons) are compared with those of experiments (squares), and the relative differences of pressure for DIA and EEA are shown in (b) and (c) respectively.

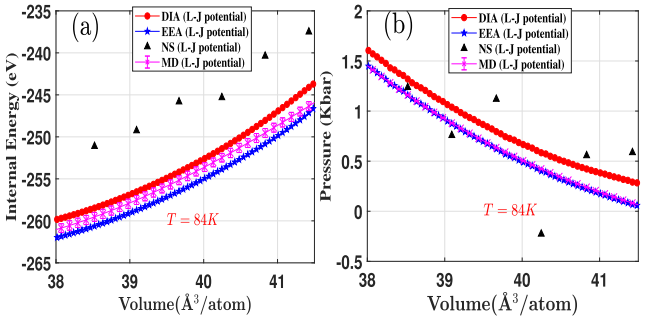

Figure 8. For the isothermal process of solid Ar with atomic volumes larger than 38 Å^3/atom at 84 K, the internal energy (a) and pressure (b) obtained by DIA (red circles), EEA (blue pentagons), NS (black triangles) and MD simulations (magenta crosses), where the results of NS are the averages over 10 times simulations.

Considering that the isochoric EOSs of solid Ar with atomic volumes ranging from 35.54 to 38.75 Å^3/atom have been obtained experimentally [72] and L-J potential is regarded as to well characterize the interatomic interactions of inert gas, we applied DIA and EEA with a model consisting of 32000 Ar atoms arranged in fcc structure to calculate the pressure (P) to be compared to the experimental ones ($P_{\rm exp}$). NS was not performed here because of too much computational cost. As shown in figure 7, the relative difference of pressure defined by RDP($= |(P - P_{\rm exp})/P_{\rm exp}|$) for DIA in most cases is below 5%, while the RDP of EEA for atomic volume of 35.54 and 36.74 Å^3/atom is significantly larger than 5%. In considerations of the experimental fluctuations of about 3% ($\pm$50 Bar) [73] and inaccuracy of the L-J potential applied, the pressures obtained by either DIA or EEA coincides quite well with the experiments.

We further validated the two approaches at the larger atomic volume zone from 38–40 Å^3/atom, and the derived isothermal EOSs are shown in figure 8 along with results of MD simulations and NS sampling. The considered system contains 4000 Ar atoms for DIA, EEA and MD simulations while 500 atoms for NS sampling due to its huge computational cost and the internal energy of NS sampling shown in figure 8(a) is multiplied by 8 times. Compared with DIA, EEA again exhibits more accuracy as the density decreases, especially for the pressure calculations. On the other hand, results of NS sampling does not coincide with those of MD simulations, and, for the pressure, show large divergence.

3.3. *For isomers of* C_{60} *molecule*

For a cluster consisting of 60 carbon atoms, the most appealing impression may be the discovery of buckminsterfullerene (BF) with a football-cage structure [74], and the followed investigations revealed that there exists a bunch of C_{60} isomers besides BF, such as those introduced by the Stone–Wales (SW) rearrangement [75]. For a long time, researches [76–78] have been attempting to answer the very questions whether the isomers are able to survive in realistic systems at finite temperatures and what the probability relative to BF is. To answer that, the most reasonable argument should be the ratio of the PF of an isomer ($\mathcal{Z}_{\rm IS}$) to that of BF ($\mathcal{Z}_{\rm BF}$), while to our best knowledge, no such theoretical works have been tried out. Among all the isomers, the stack-1 SW (SW1) isomer (see bottom in figure 9(a)) has the lowest potential energy, which is ~ 0.6 eV higher than that of BF [78] when using many-body Brenner potential [79]. Here DIA was applied to calculate $\mathcal{P} = \mathcal{Z}_{\rm SW1}/\mathcal{Z}_{\rm BF}$ with Brenner potential [79] to determine the relative surviving probability of SW1 in a temperature range from 100 K to 2500 K.

To implement DIA, we firstly determined the MSS of the BF and the SW1 isomer by the Polak–Ribiere conjugate gradient algorithm. For the MSS of BF as shown in the top panel of figure 9(a), each atom is shared by two hexagons and one pentagon, indicating that all the atoms are geometrically equivalent and thus only one atom is enough to calculate the $\mathcal{Z}_{\rm BF}$. For an arbitrary atom, the potential U' along its three Cartesian coordinates should obviously not be the same, so $\mathcal{L}_x$, $\mathcal{L}_y$ and $\mathcal{L}_z$ has to be calculated respectively and equation (16) was applied. The selected atom was moved step by step away from the equilibrium site by 0.5 Å with an interval of 0.0001 Å along its Cartesian X-axis (or Y, Z-axis), to obtain the corresponding potential-energy curves, $U'(X)$ (or $U'(Y)$, $U'(Z)$), during which, the other two coordinates and all the other atoms were kept fixed. Figure 9(b) shows the internal energy E of BF derived from the PF with the atom labeled by No. 1 in the top panel of figure 9(a) was selected to calculate $\mathcal{Z}_{\rm BF}$.

As a comparison, MD simulations with the same Brenner potential were performed via the LAMMPS code [70] to calculate the internal energy and the Nose–Hoover algorithm [71] for canonical ensemble was employed with a time step of 0.1 fs. The systems were allowed to relax 20 ps initially and continued to run for another 50 ps, during which averages of E were recorded in every 10 fs. As shown in figure 9, the internal energy E derived from $\mathcal{Z}_{\rm BF}$ are in an excellent agreement with

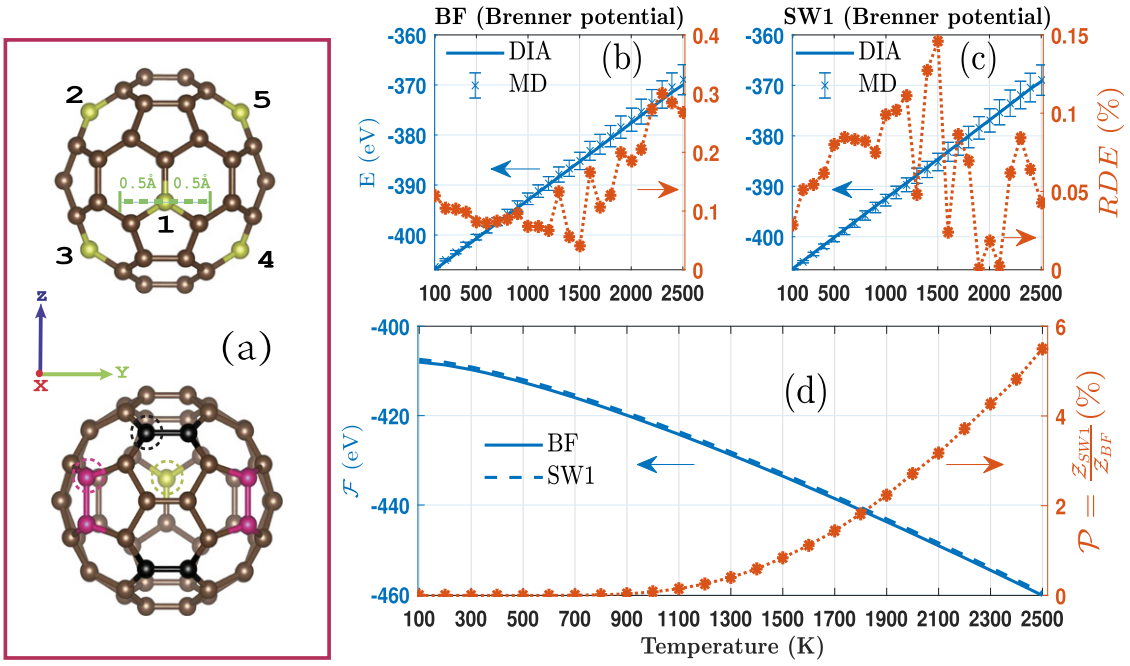

Figure 9. MSSs of BF (top) and SW1 (bottom) of C_{60} (a), and internal energies (solid lines) derived from $\mathcal{Z}_{\rm BF}$ (b) and $\mathcal{Z}_{\rm SW1}$ (c) were compared to those obtained by MD simulations (crosses) with error bars representing the standard deviations. The FEs ($\mathcal{F}$) of the two molecules and the relative probability $\mathcal{P} = \mathcal{Z}_{\rm SW1}/\mathcal{Z}_{\rm BF}$ of SW1 isomer are shown in (d).

the MD simulations and the RDE is smaller than 0.4% for the temperature up to 2500 K. It should be noted that, based on the mathematical basis, the calculation results of DIA should be *independent* of how the directions of the Cartesian coordinates are chosen. To confirm this, we arbitrarily selected four more atoms, labeled by No. 2–5 in the top panel of figure 9(a), to calculate the $\mathcal{Z}_{\rm BF}$ respectively, showing that the internal energy obtained from any one of the five atoms are nearly the same (see detailed data listed in supplementary information).

For the MSS of SW1 isomer shown in the bottom panel of figure 9(a), atoms were divided into three groups, where the first group is the atoms shared by two hexagons and one pentagon (colored in brown), the second one is the atoms shared by one hexagon and two pentagons (colored in magenta), and the last one is the atoms shared by three hexagons (colored in black). Accordingly, equation (17) was used to calculate the $\mathcal{Z}_{\rm SW1}$, and an arbitrary atom in each group, denoted by dashed circles in the bottom panel of figure 9(a), was selected to obtain the corresponding potential-energy curves respectively. The selected atoms were moved 0.5 Å step by step in positive and negative direction of the X-axis (or $U'(Y)$, $U'(Z)$), and 10^4 potential energies were recorded to obtain the corresponding potential-energy curves. As shown in figure 9(c), the RDE of $\mathcal{Z}_{\rm SW1}$ is smaller than 0.15% for the whole temperature range. In addition, we also repeated the calculation with selecting different atoms in the three groups and the obtained results are nearly the same as that shown in figure 9(c) (see detailed data listed in supplementary information).

Since the difference between FE for BF and SW1 is quite small (figure 9(d)), it is difficult to conclude whether BF is more probable than SW1 in the temperature range from 100 to 2500 K, while the ratio of PF, $\mathcal{P} = \mathcal{Z}_{\rm SW1}/\mathcal{Z}_{\rm BF}$, illustrates that the probability for SW1 to survive at low temperatures is negligible and there is a considerable chance for the isomer to form at higher temperatures. This result qualitatively agrees with previous results by MD simulations [78].

4. Summary

By testing the DIA and EEA using different potentials in high/low-density systems, we confirmed that DIA specializes in dealing with high-density or high-pressure systems but has the intrinsic shortage to deal with the low-density and high-temperature cases, because the approximation of equation (15) would gradually become invalid under those circumstances. On the other hand, EEA overcomes such a limitation of DIA and behaves much better in the situations with lower density while it may be less accurate than DIA under the extreme high-pressure conditions. As to the efficiency, the major computational cost of both DIA and EEA are the same which is to obtain the potential-energy curve U'. According to our previous comparisons [43], DIA works at least 4 orders faster than state-of-the-art numerical algorithm and about an order more precise. Such an efficiency makes it possible for both DIA and EEA not only to calculate PF of condensed systems consisting of over ten thousand of particles on desktop computers when using empirical potential, but also to implement more accurate *ab initio* methods.

It should be also interesting to compare the calculation efficiency of the MD simulations and DIA (or EEA). First of all, the CPU time consumed by DIA (EEA) is the time for calculating the curve of U', which is about 20 min using one CPU core of a desktop Intel i9-7900X, as an example for the

Cu system consisting of 4000 atoms characterized by the TB potential, and all the thermodynamics functions at any temperature, including the entropy and FE, can be obtained in several seconds using the same CPU. While MD simulations must be performed for 2×10^5 steps or more to do the statistical averages of the internal energy or pressure, and in each step the CPU time is spent on computing the force for each atom, which lasted for about 2, 100 min, ~ 1.5 days, for the same Cu system. Even so, the results obtained by the MD simulations are just only for one single given temperature and much more CPU time is needed for the simulations at other temperature conditions. Secondly, MD simulations can hardly produce either the entropy or FE to predict the probability of a given atomic configuration, which is why approaches must be developed to solutions of PF.

In conclusion, we established two independent approaches to PF of condensed systems, DIA and EEA, and the accuracy was strictly validated by vast MD simulations for condensed Cu, solid Ar, C_{60} clusters, and by experiments of solid Cu and Ar. We showed that EEA compensates the shortage of DIA for the systems with lower density while DIA performs better and better with increases of mass density. The ultrahigh efficiency enables the two methods to implement *ab initio* energy calculations, which is the first time for the computations of PF of bulkmaterials. The new approaches will find its vast applications in investigating thermodynamic properties of macroscopic condensed matters and large molecules which highly relates to designing novel material, predicting various phase transitions and parameter-free EOS under extreme conditions.

Acknowledgments

This work is supported by National Natural Science Foundation of China under Grant No. 21727801.

Appendix A. Derivations of solutions to $\mathcal{Z}$ and E

The scaled entropy of the interacting system, $\mathcal{S}'(\beta)$, is

$$\mathcal{S}'(\beta) = \ln\ \mathcal{Z} - \beta\frac{\partial}{\partial\beta}\ln\ \mathcal{Z}. \tag{A.1}$$

The general solution of $\mathcal{Z}$ is to solve the equation

$$\ln\ \mathcal{Z} - \beta\frac{\partial}{\partial\beta}\ln\ \mathcal{Z} = 0, \tag{A.2}$$

and it can be simply obtained that

$$\ln\ \mathcal{Z} = C(\beta)\beta, \tag{A.3}$$

where the parameter $C(\beta)$ is to be determined. The special solution of $\mathcal{Z}$ is obtained by inserting equation (A.3) into equation (A.1) as

$$\frac{\partial C(\beta)}{\partial\beta} = \frac{\mathrm{d}C(\beta)}{\mathrm{d}\beta} = \mathcal{S}'(\beta). \tag{A.4}$$

The expressions of parameter $C(\beta)$ and $\ln\ \mathcal{Z}$ thus are

$$C(\beta) = -\int_{\beta_0}^{\beta}\frac{\mathcal{S}'(\eta)}{\eta^2}\,\mathrm{d}\eta + C_0, \tag{A.5}$$

$$\ln\ \mathcal{Z} = \beta\left(C_0 - \int_{\beta_0}^{\beta}\frac{\mathcal{S}'(\eta)}{\eta^2}\,\mathrm{d}\eta\right). \tag{A.6}$$

The expression of internal energy $E = -\partial\ \ln\ \mathcal{Z}/\partial\beta$ becomes

$$\begin{aligned} E &= -C_0 + \frac{\mathcal{S}'(\beta)}{\beta} + \int_{\beta_0}^{\beta}\frac{\mathcal{S}'(\beta)}{\eta^2}\,\mathrm{d}\eta \\ &= -C_0 + \frac{\mathcal{S}'(\beta)}{\beta} - \left(\frac{\mathcal{S}'(\eta)}{\eta}\Big|_{\beta_0}^{\beta} - \int_{\beta_0}^{\beta}\frac{1}{\eta}\,\mathrm{d}\mathcal{S}'\right) \\ &= -C_0 + \frac{\mathcal{S}'(\beta_0)}{\beta_0} + \int_{\beta_0}^{\beta}\frac{1}{\eta}\,\mathrm{d}\mathcal{S}'. \end{aligned} \tag{A.7}$$

ORCID iDs

Bo-Yuan Ning https://orcid.org/0000-0002-7451-8828
Xi-Jing Ning https://orcid.org/0000-0003-3646-3165

References

[1] Chipot C and Pohorille A (ed) 2007 *Free Energy Calculations: Theory and Applications in Chemistry and Biology* (Berlin: Springer)
[2] Stacey F D 2005 *Rep. Prog. Phys.* **68** 341
[3] Ross M and Young D A 1993 *Annu. Rev. Phys. Chem.* **44** 61–87
[4] Monson P A and Kofke D A 2000 *Adv. Chem. Phys.* **115** 113
[5] Martynov G A 1999 *Phys. Usp.* **42** 517
[6] Ushcats M V, Bulavin L A, Sysoev V M, Bardik V Y and Alekseev A N 2016 *J. Mol. Liq.* **224** 694–712
[7] Mayer J and Montroll E 1941 *J. Chem. Phys.* **9** 2–16
[8] Wu Q, He B, Song T, Gao J and Shi S 2016 *Comput. Mater. Sci.* **125** 243–54
[9] Sanchez J M 2010 *Phys. Rev.* B **81** 224202
[10] Mueller T and Ceder G 2010 *Phys. Rev.* B **82** 184107
[11] Ballard A J, Martiniani S, Stevenson J D, Somani S and Wales D J 2015 *Wiley Interdiscip. Rev.: Comput. Mol. Sci.* **5** 273–89
[12] Laio A and Parrinello M 2002 *Proc. Natl Acad. Sci. USA* **99** 12562–6
[13] Barducci A, Bussi G and Parrinello M 2008 *Phys. Rev. Lett.* **100** 020603
[14] Barducci A, Bonomi M and Parrinello M 2011 *WIREs Comput. Mol. Sci.* **1** 826–43
[15] Laio A and Gervasio F L 2008 *Rep. Prog. Phys.* **71** 126601
[16] Valsson O, Tiwary P and Parrinello M 2016 *Annu. Rev. Phys. Chem.* **67** 159–84
[17] McCarty J and Parrinello M 2017 *J. Chem. Phys.* **147** 204109
[18] Mendels D, Piccini G and Parrinello M 2018 *J. Phys. Chem. Lett.* **9** 2776–81
[19] Zhang Y-Y, Niu H, Piccini G, Mendels D and Parrinello M 2019 *J. Chem. Phys.* **150** 094509
[20] Valsson O and Parrinello M 2014 *Phys. Rev. Lett.* **113** 090601
[21] Jarzynski C 1997 *Phys. Rev. Lett.* **78** 2690–3
[22] Moustafa S G, Schultz A J and Kofke D A 2015 *Phys. Rev.* E **92** 043303
[23] Berg B A and Neuhaus T 1991 *Phys. Lett.* B **267** 249–53
[24] Wang F and Landau D P 2001 *Phys. Rev. Lett.* **86** 2050–3

[25] Singh S, Chopra M and de Pablo J J 2012 *Annu. Rev. Chem. Biomol. Eng.* **3** 369–94
[26] Li J T, Ning B Y, Zhuang J and Ning X J 2016 *Chin. Phys.* B **26** 030501
[27] Shell M S, Debenedetti P G and Panagiotopoulos A Z 2002 *Phys. Rev.* E **66** 056703
[28] Skilling J 2004 *AIP Conf. Proc.* **735** 395–405
[29] Pártay L B, Bartók A P and Csányi G 2010 *J. Phys. Chem.* B **114** 10502–12
[30] Nielsen S O 2013 *J. Chem. Phys.* **139** 124104
[31] Wilson B A, Gelb L D and Nielsen S O 2015 *J. Chem. Phys.* **143** 154108
[32] Pártay L B, Bartók A P and Csányi G 2014 *Phys. Rev.* E **89** 022302
[33] Do H, Hirst J D and Wheatley R J 2011 *J. Chem. Phys.* **135** 174105
[34] Coe J D, Sewell T D and Shaw M S 2009 *J. Chem. Phys.* **131** 074105
[35] Baldock R J N, Pártay L B, Bartók A P, Payne M C and Csányi G 2016 *Phys. Rev.* B **93** 174108
[36] Do H and Wheatley R J 2013 *J. Chem. Theory Comput.* **9** 165–71
[37] Do H and Wheatley R J 2016 *J. Chem. Phys.* **145** 084116
[38] Do H, Hirst J D and Wheatley R J 2012 *J. Phys. Chem.* B **116** 4535–42
[39] Burkoff N S, Várnai C, Wells S A and Wild D L 2012 *Biophys. J.* **102** 878
[40] Baldock R J N, Bernstein N, Salerno K M, Pártay L B and Csányi G 2017 *Phys. Rev.* E **96** 043311
[41] Bolhuis P G and Csányi G 2018 *Phys. Rev. Lett.* **120** 250601
[42] Liu Y-P, Ning B-Y, Gong L-C, Weng T-C and Ning X-J 2019 *Nanomaterials* **9** 978
[43] Gong L-C, Ning B-Y, Weng T-C and Ning X-J J 2019 *Entropy* **21** 1050
[44] Oganov A R and Glass C W 2006 *J. Chem. Phys.* **124** 244704
[45] Wales D J and Scheraga H A 1999 *Science* **285** 1368–72
[46] Deaven D M and Ho K M 1995 *Phys. Rev. Lett.* **75** 288–91
[47] Wang Y, Lv J, Zhu L and Ma Y 2010 *Phys. Rev.* B **82** 094116
[48] Zhang Q and Buch V 1990 *J. Chem. Phys.* **92** 5004–16
[49] Ye X-X, Ming C, Hu Y-C and Ning X-J 2009 *J. Chem. Phys.* **130** 164711
[50] Gong L-C, Ning B-Y, Ming C, Weng T-C and Ning X-J 2020 *J. Phys.: Condens. Matter* **33** 085901
[51] Watanabe M and Reinhardt W P 1990 *Phys. Rev. Lett.* **65** 3301–4
[52] Cleri F and Rosato V 1993 *Phys. Rev.* B **48** 22–33
[53] Verlet L 1967 *Phys. Rev.* **159** 98–103
[54] Allen M P and Tildesley D J 1987 *Computer Simulation of Liquids* (Oxford: Oxford University Press)
[55] Louwerse M J and Baerends E J 2006 *Chem. Phys. Lett.* **421** 138–41
[56] Thompson A P, Plimpton S J and Mattson W 2009 *J. Chem. Phys.* **131** 154107
[57] Tsai D H 1979 *J. Chem. Phys.* **70** 1375–82
[58] Binder K, Block B J, Virnau P and Tröster A 2012 *Am. J. Phys.* **80** 1099–109
[59] Kraus R G, Davis J P, Seagle C T, Fratanduono D E, Swift D C, Brown J L and Eggert J H 2016 *Phys. Rev.* B **93** 134105
[60] Dewaele A, Loubeyre P and Mezouar M 2004 *Phys. Rev.* B **70** 094112
[61] Agrawal P M, Rice B M and Thompson D L 2002 *Surf. Sci.* **515** 21–35
[62] Kresse G and Furthmüller J 1996 *Comput. Mater. Sci.* **6** 15–50
[63] Kresse G and Furthmüller J 1996 *Phys. Rev.* B **54** 11169–86
[64] Perdew J P and Wang Y 1992 *Phys. Rev.* B **45** 13244–9
[65] Perdew J P, Burke K and Ernzerhof M 1996 *Phys. Rev. Lett.* **77** 3865–8
[66] Monkhorst H J and Pack J D 1976 *Phys. Rev.* B **13** 5188–92
[67] Hacene M, Anciaux-Sedrakian A, Rozanska X, Klahr D, Guignon T and Fleurat-Lessard P 2012 *J. Comput. Chem.* **33** 2581–9
[68] Hutchinson M and Widom M 2012 *Comput. Phys. Commun.* **183** 1422–6
[69] Maintz S, Eck B and Dronskowski R 2011 *Comput. Phys. Commun.* **182** 1421–7
[70] Plimpton S 1995 *J. Comput. Phys.* **117** 1–19
[71] Evans D J and Holian B L 1985 *J. Chem. Phys.* **83** 4069–74
[72] Lewis W F, Benson D, Crawford R K and Daniels W B 1974 *J. Phys. Chem. Solids* **35** 383–91
[73] Crawford R K, Lewis W F and Daniels W B 1976 *J. Phys. C: Solid State Phys.* **9** 1381
[74] Kroto H W, Heath J R, O'Brien S C, Curl R F and Smalley R E 1985 *Nature* **318** 162
[75] Heggie M I, Haffenden G L, Latham C D and Trevethan T 2016 *Phil. Trans. R. Soc.* A **374** 20150317
[76] Zhao Y, Lin Y and Yakobson B I 2003 *Phys. Rev.* B **68** 233403
[77] Bettinger H F, Yakobson B I and Scuseria G E 2003 *J. Am. Chem. Soc.* **125** 5572–80
[78] Li P and Ning X-J 2004 *J. Chem. Phys.* **121** 7701–7
[79] Brenner D W, Shenderova O A, Harrison J A, Stuart S J, Ni B and Sinnott S B 2002 *J. Phys.: Condens. Matter* **14** 783–802